International Journal of Microwave and Wireless Technologies

cambridge.org/mrf

Multiband circularly-polarized stacked elliptical patch antenna with eye-shaped slot for GNSS applications

Ahmad Abdalrazik[1], Ahmed Gomaa[2] and Asmaa Afifi[3]

[1]Electrical Engineering Department, Faculty of Engineering, Port Said University, Port Said, Egypt; [2]National Research Institute of Astronomy and Geophysics (NRIAG), Helwan, Egypt and [3]Microstrip Circuits Department, Electronics Research Institute (ERI), El-Nozha El-Gadida, Egypt

Research Paper

Cite this article: Abdalrazik A, Gomaa A, Afifi A (2024) Multiband circularly-polarized stacked elliptical patch antenna with eye-shaped slot for GNSS applications. *International Journal of Microwave and Wireless Technologies*, 1–7. https://doi.org/10.1017/S175907872400045X

Received: 28 November 2023
Revised: 16 March 2024
Accepted: 21 March 2024

Keywords:
circular polarization; elliptical patch; GNSS; multiband antenna

Corresponding author: Ahmad Abdalrazik; Email: ahmadabdalrazik@eng.psu.edu.eg

Abstract

This paper introduces a tri-band stacked elliptical patch antenna featuring a right-handed circular polarized, designed to operate at the L2, L5, and L1 Global Navigation Satellite System bands. Initially, an elliptic patch is constructed and fed by a probe feed to generate TM_{110} and TM_{210} modes at resonance frequencies calculated using Mathieu functions. The probe position is precisely adjusted to excite the quasi-orthogonal mode of TM_{110} to generate circularly polarized (CP) waves at the L2 and L5 bands. Subsequently, an eye-shaped aperture is engraved into the elliptical patch to enhance the axial ratio (AR) beamwidth in the L2 and L5 bands and stimulate the orthogonal mode of TM_{210} to produce CP waves at the L1 band. Lastly, a stacked partially elliptical parasitic element is placed beneath the upper slotted elliptical patch to enhance the orthogonality of TM_{210} surface current versions and thus improve the AR beamwidth at the L1 band. The proposed antenna shows low reflection coefficient values at 1.12–1.33 (L2/L5), and 1.5–1.66 GHz (L1). The AR beamwidths are 133/213°, 167/163°, and 36/103° at two orthogonal cutplanes at L5, L2, and L1 bands, respectively. The antenna also has decent gains of 6–6.9 dBic across the three bands.

Introduction

The Global Navigation Satellite System (GNSS) has changed the way the world operates. It provides a fast and accurate method for navigating, measuring speed, and determining a location for worldwide applications. Like all other communication systems, continuous modernization and upgrading are necessary for the GNSS to enhance its robustness and efficiency. Since the antenna element is the first part of any GNSS receiver device that is responsible for receiving wireless satellite signals, it deeply impacts the performance of the whole GNSS. To operate effectively, it must meet certain specifications [1]. It should exhibit low reflection coefficient values at as many GNSS frequency bands as possible. The antenna should also provide high-gain forward patterns and minimize signals received from other directions to reduce interference and errors from multi-path signals. Additionally, GNSS antennas are best operated in right-hand circular polarization (RHCP) mode since this helps mitigate issues caused by multi-path signals, polarization mismatch, and distortions due to transmitter–receiver respective orientations mismatch [2].

Many modern GNSS antennas have been suggested to address these considerations [3–9]. For example, Sun et al. [3] introduced a specialized antenna operating specifically within the GPS L1 band. It used a cavity-backed cross-dipole design with two curved dipoles that were printed on two perpendicular substrates. An external circuit feeds the antenna, generating CP through a corrugated metallic cavity forming the back and a curved ground plane. In [4], the authors proposed another cross-dipole design working at GNSS L1 bands. CP waves are obtained by curving the dipole arms, changing their lengths, and adjusting the spacing between them and the metallic ground plane. Another antenna for GNSS applications was introduced in [5], showcasing a printed quadrifilar helix antenna capable of operating RHCP waves over dual GPS bands, L1 and L2.

Driven by the continuous demand for modernization and upgrading GNSS, recent studies started to explore and assess the utilization of the new L5 band in GNSS, where several benefits were found, such as higher received signal power, improved robustness and energy effectiveness [10–12]. In fact, it was shown that the utilization of the L5 band enhances positioning reliability, accuracy, and precision of the GNSS receivers [12]. Modern designs of GNSS antennas in commercial and industrial applications have started incorporating L5 frequency band, with the ArduSimple™ GNSS antenna being one example [13]. However, only a limited number of studies have included the L5

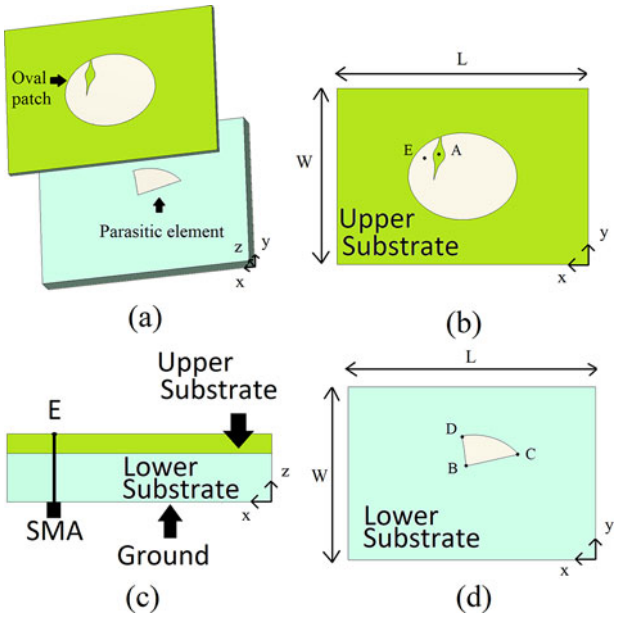

Figure 1. Proposed antenna structure. All dimensions are in mm. A = (85.1, 62.2, 19.2), B = (75, 54.6, 14.4), C = (44.9, 61.4, 14.4), D = (77.6, 72.1, 14.4), E = (94.6, 61.9, 19.2), L = 143.4, and W = 100.5. (a) Exposed 3D view. (b) Top view of the upper layer. (c) Top view of the lower layer. (d) Side view of the full structure.

GPS band in their designs [14, 15]. The few that do tend to have very narrow half-power beamwidth (HPBW) or axial-ratio-beamwidth patterns, or only support two GNSS bands.

This paper proposes a new design of an elliptical stacked triple-band GNSS antenna with an eye-shaped slot engraved in it. Unlike many previous works, our antenna produces RHCP at the three bands L1, L2, and L5 of the GNSS. Operating over multiple bands offers benefits such as improved ionosphere error correction in real-time kinematic (RTK) applications and simpler RF front-end design [1, 6]. Also, the presented antenna achieves more bands of the GNSS without needing bulky backing cavities, external feed networks, or a 3D complicated fabrication design of curved dipole arms, as required in some other designs [3–7]. It uses printed circuit board technology for ease of fabrication and cost reduction over helix/wire antennas [5]. The antenna demonstrates low S_{11} values over the L2/L5 and L1 GNSS frequency bands. Its HPBWs/axial ratio (AR) beamwidths at two orthogonal cutplanes are (133/213)°/(94/102)°,(167/163)°/(96/96)°, and (36/103)°/(86/73)° for L5, L2, and L1 respectively. The antenna also has decent gains of 6–6.9 dBic across the three bands.

Proposed antenna

Antenna structure

The proposed antenna, illustrated in Figure 1, comprises upper and lower FR4 substrates arranged in a stacked manner with a dielectric constant of 4.3 and an area of 143.4 × 100.5 mm^2, where the thicknesses of the upper and lower substrates are 4.8 and 14.4 mm, respectively. Both substrates possess an elliptical patch on the top, with dimensions of 31.1 mm for the major axis and 24.8 mm for the minor axis. Assuming the upper patch's center is at the origin, the lower patch center is positioned at the point (0.7, −2.5) mm. Additionally, an area along the lines of BC and BD is eliminated from the lower patch metal, as depicted in Figure 1. This stacked

Table 1. Summary of parameters shown in Figure 1. All dimensions are in mm

Point A	(85.1, 62.2, 19.2)
Point B	(75, 54.6, 14.4)
Point C	(44.9, 61.4, 14.4)
Point D	(77.6, 72.1, 14.4)
Point E	(94.6, 61.9, 19.2)
Length L	143.4
Width W	100.5

design is fed by a probe at point E. Furthermore, an eye-shaped slot is engraved in the upper patch of metal, centered at point A, following the two-dimensional Gielis generalized super-ellipse formula [16], as displayed in the same figure.

$$r(\varphi) = \left(\left| \frac{\cos\left(\frac{m\varphi}{4}\right)}{a} \right|^{n_2} + \left| \frac{\sin\left(\frac{m\varphi}{4}\right)}{b} \right|^{n_3} \right)^{-\frac{1}{n_1}}, \quad (1)$$

where φ is the circular coordinate angle measured from the x-axis, and m, n_1, n_2, n_3, a, and b are all positive constants. The eye slot is characterized by the parameters $m = 4.1952$, $n_2 = 8.4586$, $n_3 = 20.3611$, $n_1 = 23.7125$, $a = 30.9770$, and $b = 22.8148$. The dimensions are summarized in Table 1.

Modes analysis

The cavity model can be used to analyze elliptical patch antennas, describing the longitudinal wave equation for TM^z modes in elliptical coordinates, ξ and η, as follows [17]:

$$\frac{1}{\rho^2\left(\cosh^2\xi - \cos^2\eta\right)}\left(\frac{\partial^2 E_z}{\partial \xi^2} + \frac{\partial^2 E_z}{\partial \eta^2}\right) + k^2 E_z = 0, \quad (2)$$

where $\rho = \sqrt{a^2 + b^2}$ is the focal distance of an ellipse with major and minor axes of a and b, respectively. The solution to Equation (2) is assumed to take the form $E_z = R(\xi)\Phi(\eta)$, where $\Phi(\eta)$ and $R(\xi)$ represent the angular and radial Mathieu equations. The resonant frequency for the TM^z_{mnp} mode can be obtained by:

$$f_{mnp} = \frac{v}{2\pi}\sqrt{\frac{4q_{mn}}{\rho^2} + \left(\frac{p\pi}{d}\right)^2}, \quad (3)$$

where v is the velocity of the wave propagating inside a substrate of thickness d. The parameter q_{mn} represents the nth root of the m-degree Radial Mathieu function, and it can be found by solving the transcendental equation,

$$R_m(q, \xi_0) = 0. \quad (4)$$

Equation (4) is solved while applying the boundary condition $\xi = \xi_0$, where $\xi_0 = arctan(d(b/a))$ represents the outer side magnetic wall. It can be noted from Equation (3) that different resonant frequencies of modes can be obtained by changing elliptical patch major and minor axes, since $\rho = \sqrt{a^2 + b^2}$. Thus, one can choose appropriate values for the patch major and minor axes dimensions to obtain certain desired performance.

In our design, we choose an elliptical patch with major and minor axes measuring 31 mm and 24.8 mm, which can be shown, by Equations (2)–(4), that they generate the two modes TM_{110} and

https://doi.org/10.1017/S175907872400045X Published online by Cambridge University Press

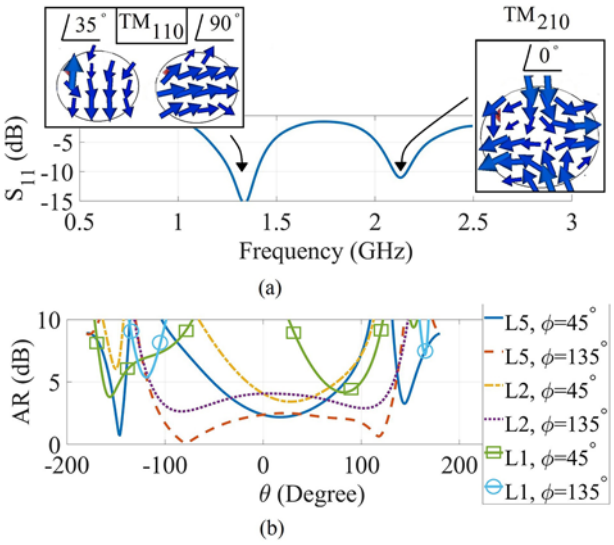

Figure 2. (a) S_{11} and (b) AR response for single layer patch antenna.

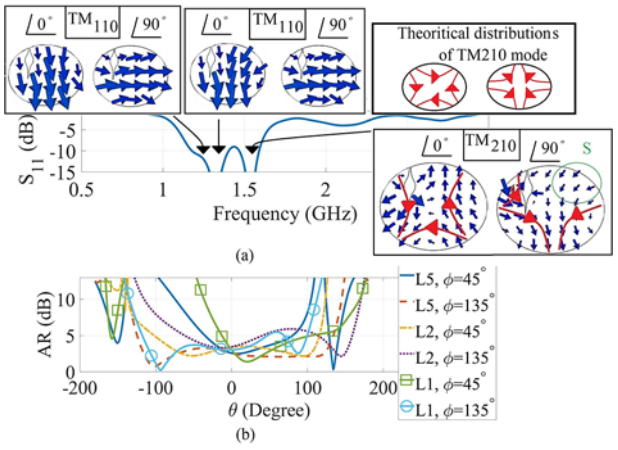

Figure 3. (a) S_{11} and (b) AR response for slotted elliptical patch antenna.

TM_{210} at frequencies of 1.1 and 2 GHz. Later in this manuscript, some structure adjustments will be carried out to fine tune the aforementioned modes to bring their resonance frequencies to GNSS bands while simultaneously widening the AR beamwidths and the HPBWs of the proposed antenna as required for GNSS applications.

Having theoretically calculated the resonance frequencies of the modes, TM_{110} and TM_{210} at 1.1 and 2 GHz, we now simulate the elliptical patch with the aforementioned dimensions to verify the theoretical results. We use CST Microwave Studio to simulate a single-layer elliptical patch, and the results are displayed in Figure 2. These simulations reveal resonance frequencies of 1.4 GHz for TM_{110} and 2.1 GHz for TM_{210}, indicating close agreement between the theoretically calculated mode frequencies and the results obtained through simulation. Additionally, Fig. 2(a) displays the surface current profiles corresponding to the TM_{110} and TM_{210} modes.

Actually, both modes, along with their orthogonal versions, can be excited with the same distributions [18, 19]. Nevertheless, the probe position impacts the phase and direction of these accompanying surface current versions. As a result, an improper position can distort their phases and directions [20]. When using an elliptic patch with major and minor axes of 31 and 24.8 mm centered at the origin, if a probe is located at point $E = (94.6, 61.9, 19.2)$, it induces two orthogonal sets of TM_{110} mode surface currents. As depicted in Figure 2, these versions are phase-delayed by approximately 55° to achieve 4 dB AR in the broadside direction at L2 band, as portrayed in Fig. 2(b). These orthogonal versions of the TM_{110} mode will be modified and exploited to enhance the CP performance in the L2 band. However, it should be noted that while the probe position at point E is suitable for producing two orthogonal versions of the TM_{110} mode surface currents, it is not entirely optimal for generating orthogonal versions of the TM_{210} mode. A more detailed discussion regarding the orthogonal surface current versions for the TM_{210} mode will be delivered.

To enhance the broadside AR performance of the L2 band elliptical patch antenna, an adjustment of the phase delay to 90° between the two orthogonal TM_{110} mode current versions is required. This is achieved by introducing an optimized eye-shaped slot at point A. The unique shape of this slot causes the y-directed TM_{110} surface currents to change direction around the slot, effectively increasing their path length. Meanwhile, the x-directed surface currents are minimally affected and undergo only slight elongation. This arrangement effectively modifies the phase delay between the two orthogonal versions of the TM_{110} mode surface currents, resulting in enhanced broadside AR performance at the L2 band. In simpler terms, the eye-shaped slot increases the phase delay of the y-directed currents more than the x-directed ones, tuning the phase delay to 90°. As a result, the slotted patch can generate CP waves in the L2 band. This is confirmed by comparing the simulated AR with and without the eye-shaped slot, as shown in Figs. 2(b) and 3(b), respectively. Furthermore, Fig. 3(b) shows that the slotted patch maintains low broadside AR values in the L5 band, signifying the preservation of orthogonality between the two versions of the TM_{110} mode current even at L5 band.

This additional slot is carefully positioned and sized to adjust the phase shift between the two orthogonal versions of the TM_{110} mode at the L5/L2 bands while also reducing the S11 at these bands. In addition, it aims to increase the current paths for the TM_{210} mode, which in turn shifts its resonant frequency to the L1 band, as shown in Fig. 3(a). Moreover, the eye-shaped slot engraved in the top patch produces two slightly distorted versions of the TM_{210} mode at the L1 band, as depicted in Fig. 3(a). In addition, Fig. 3(a) demonstrates a considerable correspondence between both the theoretical and simulated orthogonal TM_{210} surface current versions, except for a specific area referred to as S. Interestingly, the group of currents in S area deviates from the theoretical distributions expected for the TM_{210} mode. However, despite this slight distortion in the two orthogonal TM_{210} currents, CP waves are successfully generated at the L1 band. This is confirmed by the achieved broadside AR values, as illustrated in Fig. 3(b). The axial ratio beamwidths at diagonal cut-planes for L5, L2, and L1 bands are 59/195°, 106/153°, and 6/49°, respectively.

Although the elliptical slotted patch structure has achieved satisfactory AR performance, there remains potential for enhancing the AR beamwidth. The key to improving the orthogonality of the surface current versions for the TM_{210} mode has been discovered. This enhancement is achieved by incorporating a partially elliptical parasitic element beneath the upper elliptical patch, specifically in area S, resulting in a closer alignment of the surface currents with the expected theoretical distributions of the TM_{210} mode in that area. This effect is exhibited in Fig. 4(a). The addition of the parasitic patch significantly increases the AR beamwidths at the

https://doi.org/10.1017/S175907872400045X Published online by Cambridge University Press

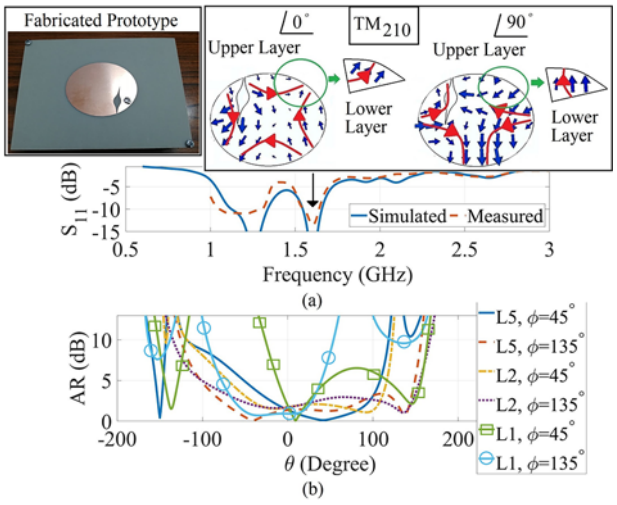

Figure 4. (a) Simulated and measured S_{11} response for the proposed antenna. (b) AR response for the proposed antenna. Inset: fabricated prototype of the antenna.

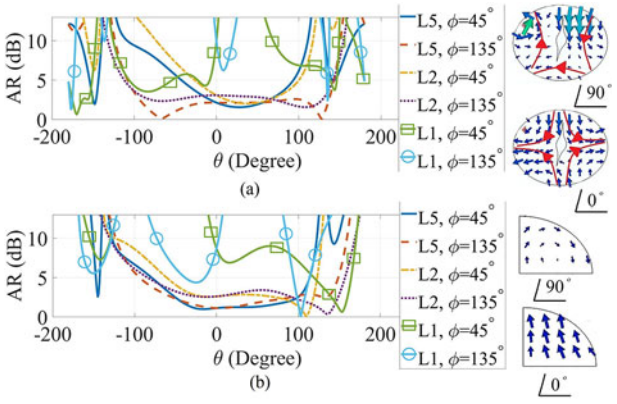

Figure 5. Simulated axial ratio response (a) with eye-shaped slot shifted to the origin, (b) with lower parasitic element shape modified.

L1 band, with an additional 30/54° at two diagonal cut planes, as demonstrated in Fig 4(b). As a result, by using the eye-shaped slot to fine-tune phase shifts between the excited modes and the parasitic element to generate surface currents that closely follow the theoretical mode patterns, CP waves are successfully generated. This advancement results in improved CP performance, as demonstrated by the AR beamwidths at two diagonal cut planes: 133/213° at the L5 band, 167/163° at the L2 band, and 36/103° at the L1 band. The fine-tuning process of the eye-shaped slot dimensions is done through parametric analysis in CST Microwave Studio software.

Parametric analysis

As discussed before, the eye-shaped aperture plays an important role in generating the circular polarization wave and hence the AR at L1, L2, and L5 bands. For further clarification, the aperture was placed in the center of the upper elliptical patch which greatly affected the broadside AR in the L1 band, in contrast to the other two bands, L2 and L5, as shown in Fig. 5(a). This is due to a significant disruption of the surface current distributions for the TM_{210}

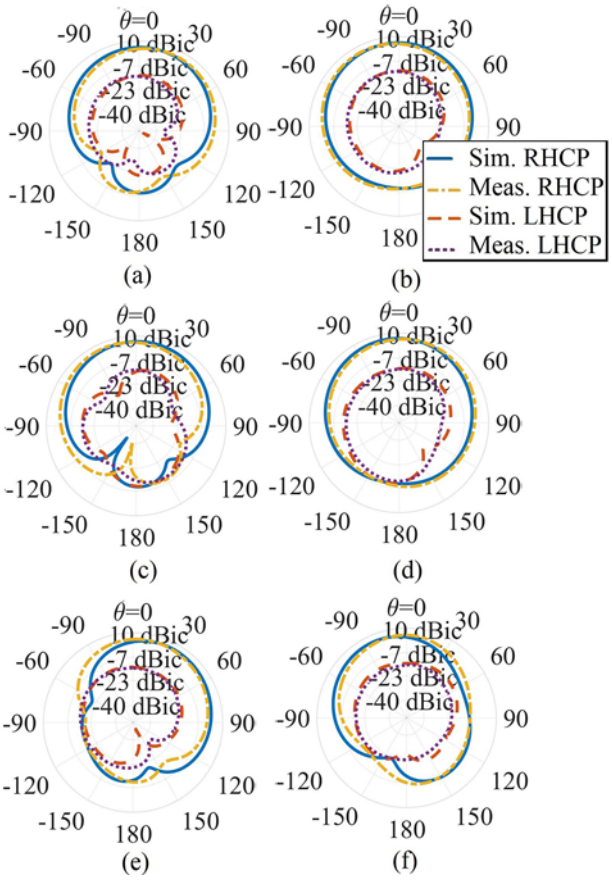

Figure 6. Simulated and measured RHCP/LCHP patterns at (a) L5, $\phi = 45°$, (b) L5, $\phi = 135°$, (c) L2, $\phi = 45°$, (d) L2, $\phi = 135°$, (e) L1, $\phi = 45°$, (f) L1, $\phi = 135°$.

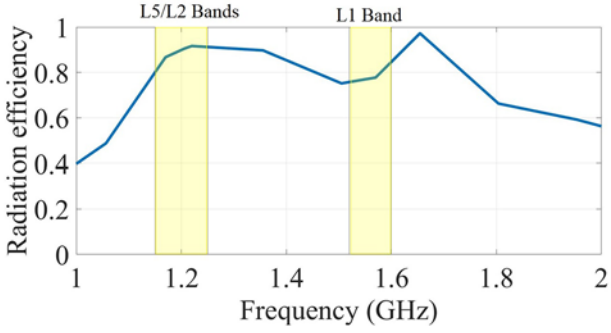

Figure 7. Radiation efficiency for the proposed antenna.

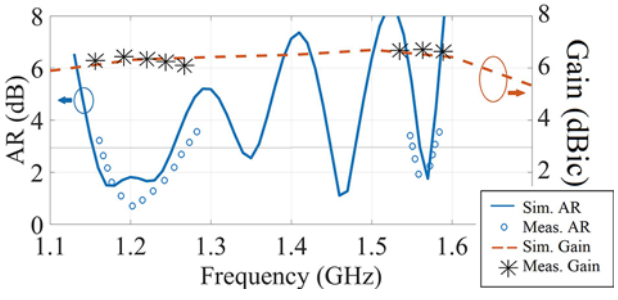

Figure 8. Simulated and measured AR and gain versus frequency.

https://doi.org/10.1017/S175907872400045X Published online by Cambridge University Press

Table 2. Performance comparison to previous works

Ref.	Smallest AR beamwidth (°)	Smallest HPBW (°)	No. of GNSS bands	Simple design/w/o ext. feed net.	Dimensions (λ_0)	Peak gain (dBic)	s_{11} Fractional band-width	AR fractional bandwidth
[5]	186, 163	126, 120	2	No	0.0709 × 0.2300 × 0.23	3.9	35.7143%	12.244% 5.12%
[6]	170, 130	108, 107	2	No	0.2854 × 0.2854 × 0.0815	3.93	0.8143% 0.8257%	NA
[4]	150	148	1	No	0.8000 × 0.8000 × 0.4	3.71	13.1%	6.37%
[7]	200, 210	103, 111	2	No	0.5500 × 0.5500 × 0.2640	5.88	43.9%	20.4% 23.2%
[8]	60	60	1	Yes	0.2167 × 0.1603 × 0.0251	−1.17	22.5256%	0.26%
[3]	230	150	1	No	0.7375 × 0.7375 × 0.3442	4.69	19%	6.30%
[9]	188	30	1	Yes	0.4689 × 0.4689 × 0.0156	5.4	1.7127%	0.63%
[21]	120[a]	∼60, 55, 46	3	Yes	0.32 × 0.32 × 0.024	5.53	5.16% 3.68% 1.45%	3.19% 3.04% 2.21%
[22]	90,60	∼75, 67, 60	2	Yes	0.46 × 0.46 × 0.086	5	16% 12.5%	6.9% 0.6%
[23]	90[a]	NA	2	Yes	0.26 × 0.26 × 0.018	4.46	2.00%	1.61%
Proposed work	133, 163, 36	94, 96, 73	3	Yes	0.5019 × 0.3518 × 0.0672	6.9	21.2766% 6.2893%	8.9304% 8.9304% 2.1357%

[a]Other AR beamwidths are not discussed in the manuscripts.

mode by changing the location of the slot which in turn removes the orthogonality of the two TM_{210} mode versions. As for the L2 and L5 bands, although the slot position changes, the delay for the TM_{110} version in the x-direction is still much larger than that in the y-direction, maintaining the orthogonality of the distributions of the different versions. Besides the eye-shaped aperture, the bottom parasitic patch in area S also plays a crucial role in impacting the broadside AR at the L1 band. Therefore, when the parasitic patch shape is modified, even if the change is slight, it causes the surface current not to follow the theoretical distribution for the TM_{210} mode, which negatively affects the broadside AR at L1 band, as shown in Fig. 5(b).

Fabrication and measurements

The proposed antenna was fabricated as illustrated in Figure 4, and both the R&S®ZVB Vector Network Analyzer and anechoic chamber were used to measure the performance of the antenna to compare the measured and simulated results. According to Fig. 4(a), the measured reflection coefficient of the proposed antenna provides 10 dB bandwidths of 1.05–1.3 for (L2/L5) and 1.54–1.64 GHz for (L1) bands. As depicted in the previous figure, there is a close correspondence between the measured results and those obtained through simulation. The measured results also show that the antenna radiates with the RHCP wave as required for GNSS antennas as illustrated in Figure 6 for the measured RH and LH radiation patterns. The measured HPBWs are (95/103)°, (96/96)°, and (87/68)° at two orthogonal cut-planes, with gains of 6, 6.4, and 6.9 dBic at the three GNSS bands, L5, L2, and L1, respectively. Overall, the measured results agree closely with the simulated ones, suggesting a simple GNSS antenna configuration capable of RHCP operation across the L1, L2, and L5 frequency bands.

The performance of the suggested antenna is compared with previous research as demonstrated in Table 2. Analyzing the earlier studies indicated in the table reveals that narrower HPBW and/or AR beamwidth are invariably the result of increasing the number of operating bands. One design that has the widest AR beamwidth and HPBW, for example, is described in [3]. However, it only has one operational GNSS band. There are two operational GNSS bands, with AR beamwidth and HPBW being narrower than [3], according to other designs that have been presented [5–7]. AR beamwidths and HPBWs are relatively good, and our suggested design has the most operational GNSS bands in the same context. As previously mentioned, the large number of operating bands makes it possible to effectively correct for ionosphere errors in RTK applications and lowers the complexity of the RF front-end [1, 6].

Also, we show in Figure 7 the radiation efficiency for the proposed antenna, where it can be seen that the radiation efficiency ranges from 80% to 91% in L5/L2 bands, and ranges from 75% to 85% in the L1 band. Moreover, we show in Figure 8 simulated and measured AR and gain versus frequency. It can be seen that the proposed antenna provides a good fractional AR bandwidth of 8.93% at L5/L2 GNSS bands and 2.13% at L1 GNSS band. Also, the proposed antenna shows decent gains of 6–6.9 dBic across the three bands. The peak gain obtained is 6.9 dBic, which is a high value compared to previous works (see Table 2). Further enhancement for the proposed design gain could be obtained by placing a lower

https://doi.org/10.1017/S175907872400045X Published online by Cambridge University Press

metasurface layer which further reduces backlobe radiation [24]. The insertion of a lower metasurface layer could be considered in a future work.

Conclusion

This paper introduced a triple-band stacked elliptical patch GNSS antenna featuring an eye-shaped slot, designed for RHCP operation at the L1, L2, and L5 bands. The optimization of the dimensions and position of the eye-shaped slot facilitated the generation of CP waves across these bands. Additionally, the incorporation of a partially elliptical-shaped parasitic element beneath the elliptical patch resulted in wider AR beamwidths. The antenna was fabricated, measured, and compared to previous works, showing a high number of operating GNSS RHCP bands. The measured reflection coefficient exhibited 10 dB bandwidths of 1.05–1.3 GHz for L2/L5 and 1.54–1.64 GHz for L1 bands. At two orthogonal cut-planes, the measured HPBWs were 95/103°, 96/96°, and 87/68° for L5, L2, and L1 bands, respectively. The antenna also has decent gains of 6–6.9 dBic across the three bands. The radiation efficiency ranged from 80% to 91% in L5/L2 bands and from 75% to 85% in the L1 band. Moreover, the proposed antenna demonstrated a good fractional AR bandwidth of 8.93% at L5/L2 GNSS bands and 2.13% at the L1 GNSS band.

Funding statement. This paper is based upon work supported by Science, Technology and Innovation Funding Authority (STDF) under grant (46124).

Competing interests. The authors declare none.

References

1. **Rao BR, McDonald K and Kunysz W** (2013) *GPS/GNSS Antennas*. London: Artech House.
2. **Mak KM and Luk KM** (2009) A circularly polarized antenna with wide axial ratio beamwidth. *IEEE Transactions on Antennas and Propagation* **57**(10), 3309–3312.
3. **Sun Y-X, Leung KW and Lu K** (2017) Broadbeam cross-dipole antenna for GPS applications. *IEEE Transactions on Antennas and Propagation* **65**(10), 5605–5610.
4. **Zhang Y-Q, Qin S-T, Li X and GuoL-X** (2018) Novel wide-beam cross-dipole CP antenna for GNSS applications. *International Journal of RF and Microwave Computer-Aided Engineering* **28**(6), e21272.
5. **Liu H, Shi M, Fang S and Wang Z** (2020) Design of low-profile dual-band printed quadrifilar helix antenna with wide beamwidth for UAV GPS applications. *IEEE Access* **8**, 157541–157548.
6. **Zhong Z-P, Zhang X, Liang J-J, Han C-Z, Fan M-L, Huang G-L, Xu W and Yuan T** (2019) A compact dual-band circularly polarized antenna with wide axial-ratio beamwidth for vehicle GPS satellite navigation application. *IEEE Transactions on Vehicular Technology* **68**(9), 8683–8692.
7. **Sun Y-X, Leung KW and Ren J** (2018) Dual-band circularly polarized antenna with wide axial ratio beamwidths for upper hemispherical coverage. *IEEE Access* **6**, 58132–58138.
8. **Sakthi Abirami B, Sundarsingh EF and Harshavardhini A** (2019) A compact conformal windshield antenna for location tracking on vehicular platforms. *IEEE Transactions on Vehicular Technology* **68**(4), 4047–4050.
9. **Wang M-S, Zhu X-Q, Guo Y-X and Wu W** (2018) Compact circularly polarized patch antenna with wide axial-ratio beamwidth. *IEEE Antennas and Wireless Propagation Letters* **17**(4), 714–718.
10. **Munoz-Martin JF, Onrubia R, Pascual D, Park H, Pablos M, Camps A, Rüdiger C, Walker J and Monerris A** (2021) Single-pass soil moisture retrieval using GNSS-R at L1 and L5 bands: results from airborne experiment. *Remote Sensing* **13**(4), 797.
11. **Madry S** (2015) *Global Navigation Satellite Systems and Their Applications*. New York: Springer.
12. **Saleem T, Usman M, Elahi A and Gul N** (2017) Simulation and performance evaluations of the new GPS L5 and L1 signals. *Wireless Communications and Mobile Computing* **2017,** 7492703.
13. **ArduSimple GNSS Antennas**. https://www.ardusimple.com/ (accessed April 2022).
14. **Che J-K, Chen C-C and Locke JF** (2021) A compact cavity-backed tri-band antenna design for flush mount GNSS (L1/L5) and SDARS operations. *IEEE Antennas and Wireless Propagation Letters* **20**(5), 638–642.
15. **Hussine UU, Huang Y and Song C** (2017) A new circularly polarized antenna for GNSS applications. In *2017 11th European Conference on Antennas and Propagation (EUCAP)*. IEEE, pp. 1954–1956.
16. **Matsuura M** (2015) Gielis' superformula and regular polygons. *Journal of Geometry* **106**(2), 383–403.
17. **Gutiérrez-Vega JC, Rodrıguez-Dagnino R, Meneses-Nava M and Chávez-Cerda S** (2003) Mathieu functions, a visual approach. *American Journal of Physics* **71**(3), 233–242.
18. **Kumar C and Guha D** (2011) Nature of cross-polarized radiations from probe-fed circular microstrip antennas and their suppression using different geometries of defected ground structure (DGS). *IEEE Transactions on Antennas and Propagation* **60**(1), 92–101.
19. **Samanta S, Reddy PS and Mandal K** (2018) Cross-polarization suppression in probe-fed circular patch antenna using two circular clusters of shorting pins. *IEEE Transactions on Antennas and Propagation* **66**(6), 3177–3182.
20. **Li Q, Li W, Zhu J, Zhang L and Liu Y** (2020) Implementing orbital angular momentum modes using single-fed rectangular patch antenna. *International Journal of RF and Microwave Computer-Aided Engineering* **30**(5), e22165.
21. **Agarwal K, Nasimuddin and Alphones A** (2014) Triple-band compact circularly polarised stacked microstrip antenna over reactive impedance meta-surface for GPS applications. *IET Microwaves, Antennas & Propagation* **8**(13), 1057–1065.
22. **Nasimuddin Chen ZN and Qing X** (2010) Dual-band circularly polarized *s*-shaped slotted patch antenna with a small frequency-ratio. *IEEE Transactions on Antennas and Propagation* **58**(6), 2112–2115.
23. **Agarwal K, Guo YX and Alphones A** (2013) Dual-band circularly polarized stacked microstrip antenna over RIS for GPS applications. In *2013 IEEE International Wireless Symposium (IWS)*. IEEE, pp. 1–4.
24. **Chung KL and Kharkovsky S** (2013) Metasurface-loaded circularly-polarised slot antenna with high front-to-back ratio. *Electronics Letters* **49**(16), 979–981.

Ahmad Abdalrazik received his B.Sc. and M.Sc. degrees in Electrical Engineering from Port Said University, Egypt in 2012 and 2016, respectively. He received his Ph.D. degree from Egypt-Japan University of Science and Technology, Alexandria, Egypt, in 2020. He worked as a researcher at Kyushu University, Japan in 2019. Currently, he is an assistant professor at Port Said University. His research interests include antenna design, microwave devices, wave propagation modeling, metamaterial, and optimization.

https://doi.org/10.1017/S175907872400045X Published online by Cambridge University Press

Ahmed Gomaa Received the B.Sc. degree (Hons.) in Electronics, Communications, and Computer engineering, in 2009, the M.Sc. degree from Cairo University in Electronics, Communications, and Computer Engineering, Cairo, Egypt, in 2015, and the Ph.D. degree from the School of Electronics, Communications, and Computer Science Engineering, Egypt-Japan University of Science and Technology (E-JUST), in collaboration with Kyushu University, Japan in 2020. From 2009 to 2015, he was a Teaching Assistant at Electronics and Communication Department, IAET. In 2015, he joined National Research Institute of Astronomy and Geophysics (NRIAG), Egypt. In February 2019, he has joined the Laboratory for Image and Media Understanding (LIMU), Kyushu University, Japan, as a Special Research Student. From 2022 to 2023, he has joined the Laboratory for Image and Media Understanding (LIMU), Kyushu University, Japan, where he had a POST-DOC Fellowship. He is currently an Assistant Professor with the National Research Institute of Astronomy and Geophysics (NRIAG). His current research interests include Image & Video Processing, Computer Vision, Deep Learning, Global Navigation Satellite Systems (GNSS), Remote Sensing, Wireless Sensor Networks, Intelligent transportation systems, and Object Detection & Tracking.

Asmaa Afifi received the B.Sc. degree in Electrical Engineering from Al-Azhar University, Egypt, in 2012, the M.Sc. and Ph.D. degrees in Electronics and Communications Engineering from Egypt-Japan University of Science and Technology (E-JUST), Alexandria, Egypt, in 2017 and 2020, respectively. In 2013, she joined the Electronics Research Institute (ERI) as a research assistant with the Microstrip Circuits Department. From May to October 2022, she was a postdoctoral researcher in the Electromagnetic Engineering Laboratory with the Department of Communications Engineering, Faculty of Engineering, Tohoku University, Japan. She is currently a researcher at the Electronics Research Institute (ERI). Her primary research interests include planar, DRA, different types of antennas, microwave and millimeter wave, sensor design for breast cancer detection and materials characterization.

https://doi.org/10.1017/S175907872400045X Published online by Cambridge University Press